AD-A031 986 SAGE ACTION INC ITHACA N Y F/G 20/4
PRELIMINARY INVESTIGATION OF THE ROLE OF THE TIP VORTEX IN ROTA--ETC(U)
DEC 74 R W HALE, P TAN, R C STOWELL, L S IWAN N00014-72-C-0200

UNCLASSIFIED SAI-RR-7402 NL

| OF |
AD
A031986

END

DATE
FILMED
1-76

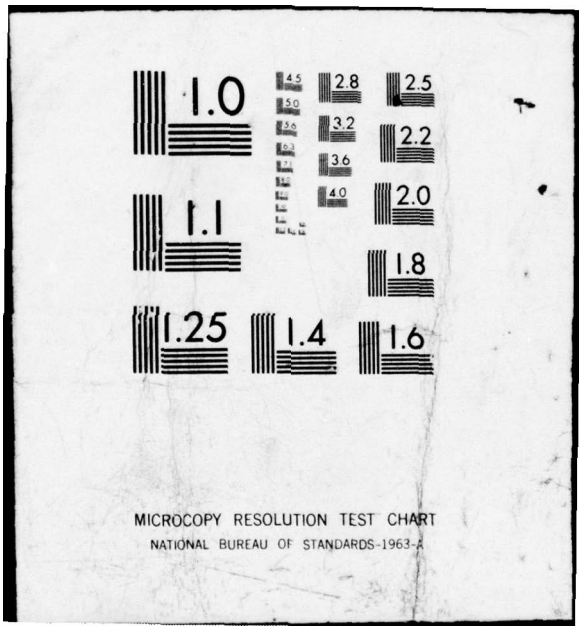
1.0
1.1
1.25
1.4
1.6
1.8
2.0
2.2
2.5
2.8
3.2
3.6
4.0
4.5
5.0
5.6
MICROCOPY RESOLUTION TEST CHART
NATIONAL BUREAU OF STANDARDS-1963-A

(14) SAI-RR-7402
December 1974

(6) PRELIMINARY INVESTIGATION OF THE ROLE OF THE TIP VORTEX IN ROTARY WING AERODYNAMICS THROUGH FLOW VISUALIZATION.

(9) Technical rept. no. 1, 1 Jan 72 – 28 Feb 73,

by

(10) R. W. Hale, P. Tan, R. C. Stowell, L. S. Iwan and D. E. Ordway

SAGE ACTION, Inc.
Ithaca, New York

(11) Dec 74

(12) 39 p.

Sponsored by:

Vehicle Technology Program, Code 211
Technology Projects Division
Office of Naval Research
Arlington, Virginia 22217

(15) Prepared under Contract N00014-72-C-0200,
NR 215-194

388 523
bpg

FOREWORD

This work was performed for the Office of Naval Research, Vehicle Technology Program, Code 211, Technology Projects Division, under ONR Contract N00014-72-C-0200. T. L. Wilson of the ONR served as technical monitor.

The authors would like to express their appreciation to the NASA Langley Research Center for the use of the V/STOL Research Wind Tunnel and, in particular, to A. D. Hammond, W. C. Sleeman, Jr., D. R. Croom and J. F. Ward for their cooperation and assistance.

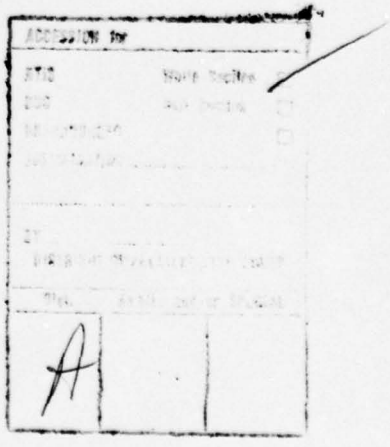

ABSTRACT

The interaction between the tip vortices and successive rotor blades is responsible for two important helicopter problems, static loss in lift and blade slap during power descent. As a step toward the solution of these problems, the objective of this investigation was to examine the flowfield about an isolated blade in rectilinear flow up to 40 chords downstream. Wind tunnel tests were carried out on the tip section of a HR2S-1 (S-56) blade in the NASA Langley V/STOL Research Wind Tunnel. Visualization of the detailed flow patterns, particularly the tip vortex and rollup in the near wake, was achieved using small, neutrally-buoyant bubbles as flow tracers. To provide adequate illumination, a new, expanded lighting arrangement was assembled from an array of searchlights. Also, a special chopper unit was designed and constructed for quantitative velocity data. Records of the flow patterns were made, both by means of still photography and a video system employing a high-sensitivity camera.

TABLE OF CONTENTS

1 INTRODUCTION

The tip vortex has received a considerable amount of attention within the past few years. This interest has been prompted by several problems encountered in the current operation of both fixed wing and rotary wing aircraft, e.g. Refs. 1 and 2. The problems, though, for these two cases are quite different in nature.

With respect to fixed wing aircraft, the trailing vortices behind large transports, particularly the new jumbo jets, persist for some distance. These vortices are strong and big enough to be potentially dangerous to smaller aircraft. Agencies such as the FAA are seeking realistic aircraft separation standards for safe operation, as well as possible means for detecting the presence of dangerous vortices. This we can classify as a *far wake problem*, which requires an understanding of the decay process.

Conversely, the tip vortex problem for rotary wing aircraft arises from the *near wake*. Under certain flight conditions, the tip vortex trailing from each blade passes near or actually impinges on the following blade. Typically, the distance between blades along the tip trajectory is 15 to 40 blade chords. The tip vortex remains tightly concentrated over these distances and this flow does not resemble the final stage of vortex decay at all.

From a Navy standpoint, the tip vortex problem associated with helicopters is naturally of more immediate concern since very large fixed wing aircraft are not carried in the inventory. The difficulties are twofold. In hover, the tip vortex is responsible for a substantial loss in lift, and during forward flight, the tip vortex may cause appreciable blade slap. A solution to either difficulty would lead to significant improvements in the operational capabilities of Navy helicopters. At the same time, a better understanding of the tip vortex phenomen might lead to better fixed wing designs, especially configurations with new lift or control innovations.

Although a lot of work has been done on the *effects* of vortex-blade interaction, little is actually known of the nature of the vortex itself. This is probably due to the complexity of the flow pattern. Its complexity almost precludes the application of conventional experimental methods. In fact, there is a legitimate question whether any kind of probe can be introduced without causing secondary flow.

The main objective of this work was to carry out an investigation specifically tailored to the formulation of a clearer picture of the role which the tip vortex plays in rotary wing aerodynamics. The key element is a new technique of flow visualization using neutrally-buoyant bubbles. This technique was

originally developed under ONR Contract N00014-68-C-0434 and has already proven[3-6] its unique capabilities, qualitatively and quantitatively.

We will begin with a more detailed discussion of the tip vortex problem for helicopters. This is followed by an outline of our overall investigation. Next, we describe the changes which we had to make in our previous flow visualization system and trace the development of the equipment involved. The reasons for the choice of the NASA Langley V/STOL Research Wind Tunnel are then presented. Finally, we cover the tests themselves, together with some preliminary results, and summarize our conclusions and recommendations.

2 THE TIP VORTEX PROBLEM FOR HELICOPTERS

It is helpful to elaborate somewhat further on the helicopter difficulties that the tip vortex causes. In the static condition, there is a strong contraction in the slipstream immediately beneath the rotor disk. The final contraction of the slipstream, the ratio of the radius of the slipstream far beneath the rotor to the radius of the rotor, is about 71% for a representative disk loading[7]. At a location only 0.2 of the radius beneath the rotor, though, the contraction is already 80%. Consequently, the vortices from the blade tips tend to linger in the rotor plane.

To show this graphically, Fig. 1 has been redrawn from Ref. 8 by D. R. Clark and A. C. Lieper. This depicts the observed tip vortex trajectory for the Sikorsky CH-53A main rotor at high lift levels. We see that the tip vortex moves inward rapidly but only goes downward slightly, passing just below Blade 2.

The close passage of the vortex to the blade produces a strong interference which affects the rotor performance drastically. The inadequacy of the available design methods to calculate the lift consistently at the static condition has been recognized for some time. Most of the work along these lines has focused on the so-called "force-free" wake analysis in order to get the proper deformation of the trailing vortices. Much progress has been made and this is fairly well in hand. Still, substantial discrepancies arise between the predicted and measured performance.

Why? It has been found that the tip vortex interference induces violent changes in the local angle of attack and leads to separation or stall. As shown in Fig. 1, the stalled area may extend over a region almost 1 1/2 chords wide in the spanwise direction. This, in turn, can cause a significant loss in lift. For example, if we take a CH-53A rotor 72' in diameter with six blades of 26" chord, the estimated loss at a lift of 45,000 lbs would be 3,000 lbs, a large fraction of the helicopter payload.

Turning to the noise difficulty, we find the details of this phenomenon do not seem to be so well defined yet. For the most part, people agree that blade slap results from blade-vortex interaction, local shock waves, or a combination of both. To get an idea of the flight conditions at which slap occurs, Fig. 2 has been taken from Ref. 9. This plot defines the combinations of airspeed and climb/descent rates that produce different levels of noise for typical 10,000 lb class helicopters.

At the far right of the figure, the helicopter is flying at or near maximum forward speed. The noise here is independent of climb or descent rates and is

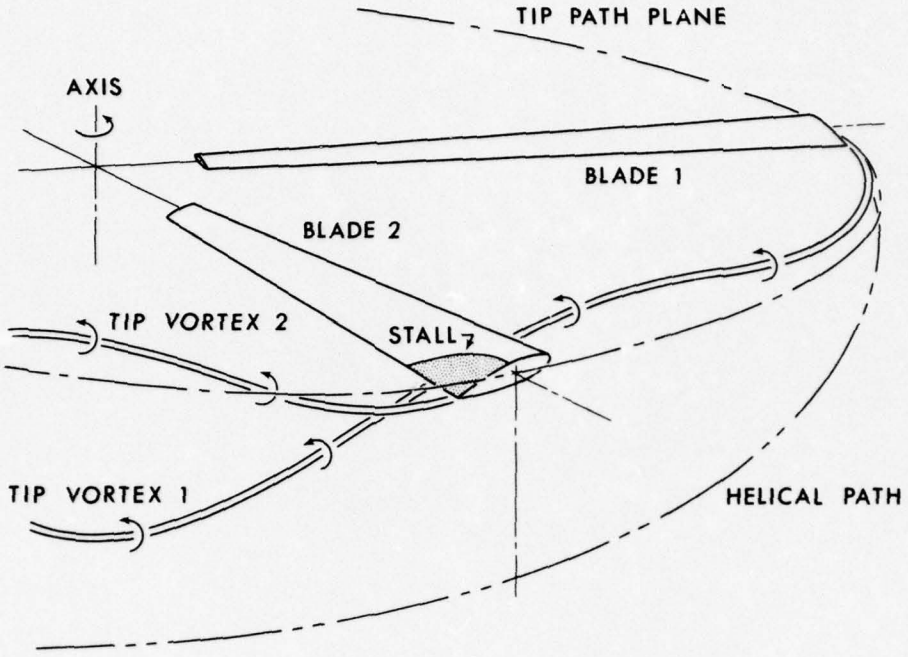

Figure 1. Typical Rotor Tip Vortex Interaction Phenomenon In Hover

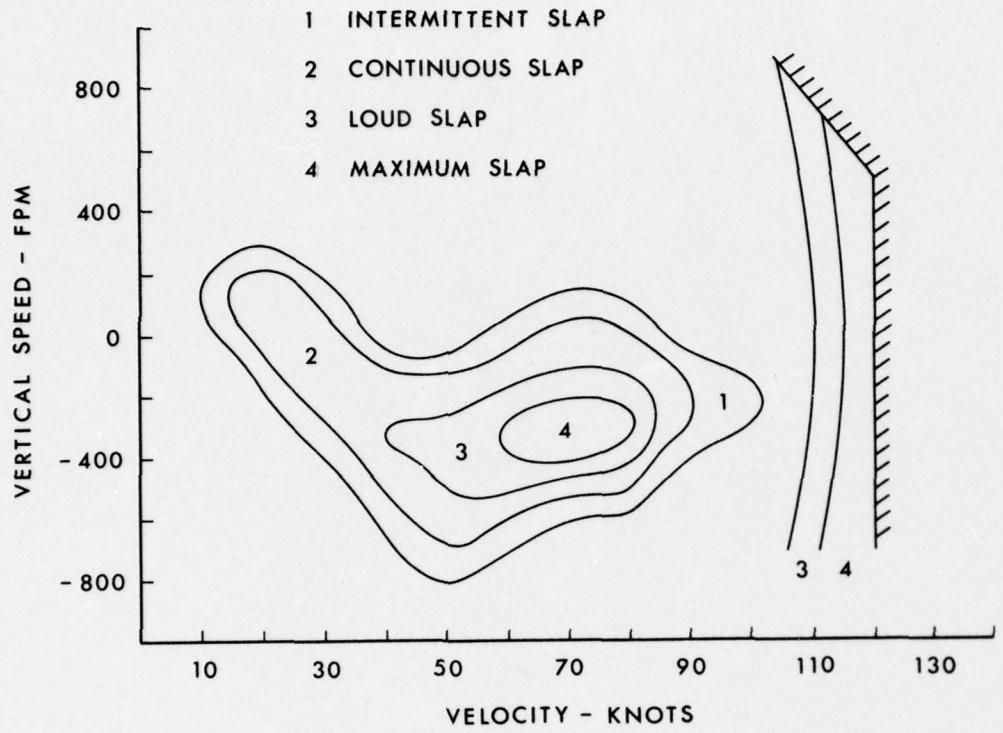

Figure 2. Contour Map Of Flight Conditions For Helicopter Blade Slap

almost certainly due to the blades entering a transonic flow condition on the advancing side. This causes shock waves to form, creating rapidly fluctuating airloads. The noise generated is very directional and propagates forward for several miles.

Maximum slap is also seen to occur during partial power descents, the condition under which the blades are most likely to interact with their own wake. The blades intersect the vortex system from the preceding blades, as in the hovering case, but more directly. Again high velocities and angles of attack are induced locally that produce compressibility and stall conditions. Since this occurs in an unsteady fashion, the airloads fluctuate rapidly and an extremely loud noise can result.

In level flight, blade slap can be intermittent or continuous, though usually not as severe as during descent. It is hard to avoid blade slap during landing manuevers because descent conditions appear to be worse. This can subject ground or ship personnel to intolerably high noise levels.

3 OUTLINE OF OVERALL INVESTIGATION

Before we can surmount these difficulties, we must go back and get a good understanding of the tip vortex itself. Such an understanding does not exist at present. As we said earlier, the difficulty is the complexity of the flow. The best way to unravel this complexity is through flow visualization.

Two tests along these lines have been carried out previously using neutrally-buoyant bubbles[6]. As opposed to smoke, cf. Ref. 10, the details of the flow are sharply defined and afford considerable insight into the associated physical mechanisms. Still, a more comprehensive investigation, both experimental and analytical, was needed.

With regard to equipment, only a modest change in the bubble generator already developed was required. In particular, a new console was designed and built to drive up to three heads simultaneously. What we really lacked was a lighting arrangement suitable for a much broader view of the flowfield, plus a chopper to obtain velocity data.

After the new lighting arrangement and chopper were completed, extensive tests were run on our existing helicopter blade model. This model is the outer portion of a HR2S-1 (S-56) blade. Both still photographs and videotapes were made. These tests were done with extreme care and thoroughness to establish a reference or "norm" for later comparisons.

From the results, we hope to improve our knowledge of the tip vortex substantially. We are especially interested in the radial inflow. This has been observed in a number of studies, but its importance has not been recognized. Since it is small relative to the tangential and axial components of flow, the radial flow is usually neglected. Yet we feel that it plays a pivotal part in sustaining the tip vortex downstream and may lead to a simple, efficient means of control.

A precedent is known in the case of *confined* vortex flows. An excellent discussion of the behavior of confined vortices is presented in Ref. 11. Basically, the radial flow through the vortex and into the core, or the radial Reynolds number, controls the vortex strength. This is the way that angular momentum is convected inwards to balance viscous dissipation. With more radial flow, the viscous core becomes smaller and the fluid particles retain their angular momentum longer, thereby producing higher peak tangential velocities. If the radial flow is cut off, the vortex dies very quickly.

Our current investigation does not resolve the question of vortex-blade interaction. It does take us, though, much closer. Subsequent efforts should be

directed toward investigation of a tandem configuration such as sketched in Fig. 3. Some recent work along these lines has been done by B. Monnerie and A. Tognet[12].

Figure 3. Tandem Blade Concept For Simulation Of Rotor Tip Vortex Interaction

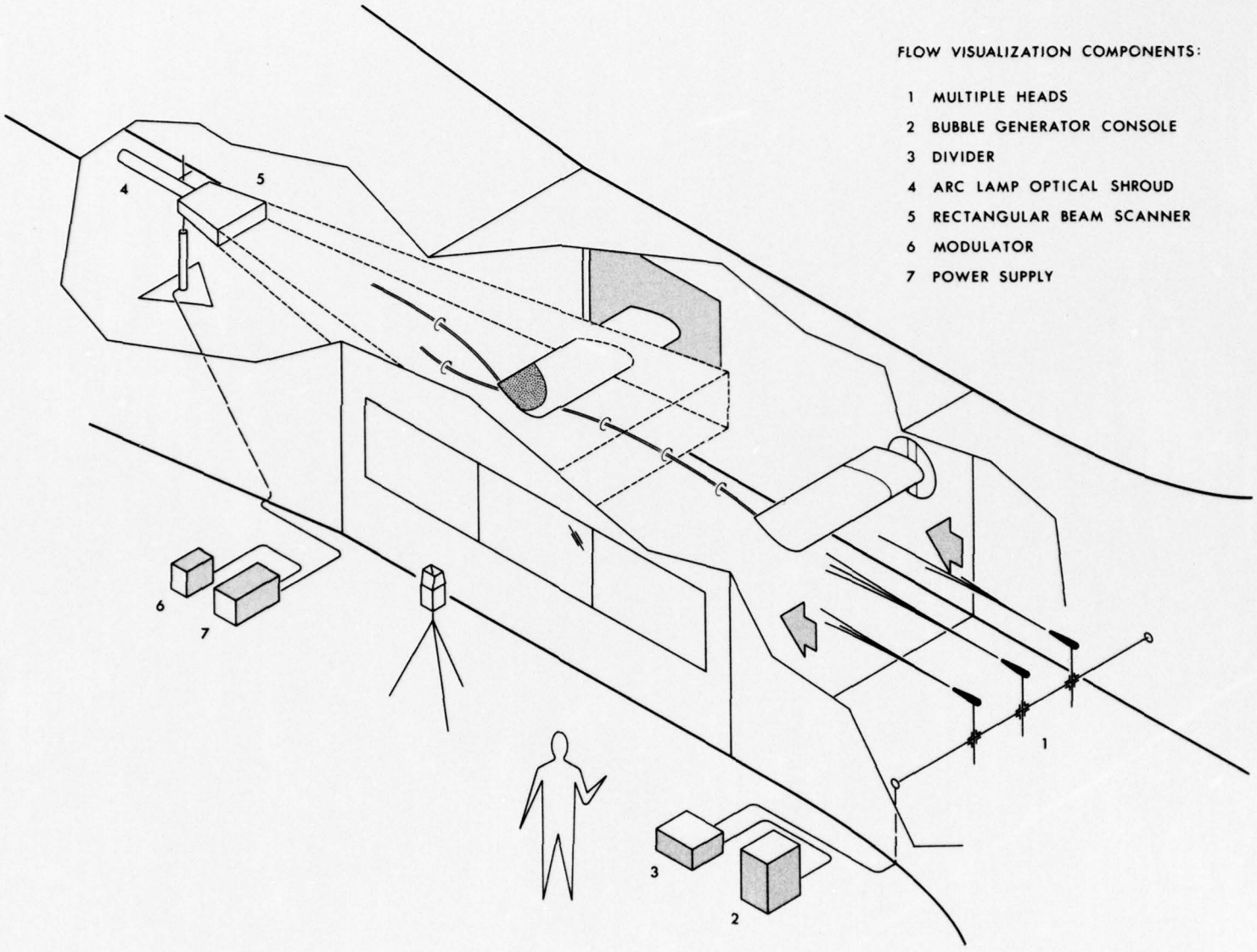

FLOW VISUALIZATION COMPONENTS:

1 MULTIPLE HEADS
2 BUBBLE GENERATOR CONSOLE
3 DIVIDER
4 ARC LAMP OPTICAL SHROUD
5 RECTANGULAR BEAM SCANNER
6 MODULATOR
7 POWER SUPPLY

4 EXPANDED LIGHTING ARRANGEMENT

In view of the preceding considerations, we decided to map out the complete flowfield as far downstream as 20 chord lengths from our rotor blade model. This dictated a lighting system that would provide much broader coverage than our previous, small xenon arc lamp[6]. Consistent with the dimensions of the model, we wanted to fill a "slab" of space about 2' x 6' x 40'.

We looked at two approaches initially. One approach was an optical scanner to sweep the beam from a single light source back and forth very rapidly through the desired space. This could be built around either a rotating prism or an oscillating mirror. However, certain problems such as divergence of the beam, continuity of the film images from the bubble highlights and the optics involved to focus the light on the scanning mirror, were very difficult. As a result, we abandoned this approach.

The other approach, which we selected instead, was a bank of multiple light sources. That is, three or four light sources could be mounted side-by-side so that the beams overlap in a composite pattern which is essentially rectangular. The only real problem was modulation for velocity measurements. If we tried to modulate electronically, as we did with our arc lamp, each source would require separate modulation. This, in turn, would require some method of synchronization. The solution was to interrupt the light entering the camera, rather than to interrupt the light source itself. The design of a mechanical chopper for this purpose is described later.

As a start, we contacted several suppliers and thoroughly examined a number of lights suitable for our multiple arrangement. Unfortunately, all of them fell into what is commonly called the "spotlight" category. These lights have a characteristic beam spread on the order of 10°. This much divergence would make it impossible to fill the slab desired.

After further investigation, we discovered that only a searchlight has a much narrower beam. The beam spread can be as small as 1° to 2°, just the amount of divergence needed. For example, in a typical installation, we would place the 2-D light source around 30', say, downstream of the slab. Altogether, then, the total distance between the source and the front of the slab would be 70'. To get a beam width of 2' at this distance, the beam spread should be 1.63°, a value right within the quoted beam spread capability.

Analysis of the specific lighting requirements was undertaken at the same time. In particular, we sought to determine the proper level of illumination E, or the amount of light falling on a unit area at any point of observation. This is measured in lumens per square foot or foot-candles. We should also know the

light flux in a unit solid angle I, which is called the luminous intensity. The appropriate units for I are lumens per steradian or candles, though it is often expressed incorrectly as the beam "candlepower". The only other quantity that we should have is the luminous flux of the beam. It is given in lumens and constitutes a constant of the beam. Either E or I can be integrated to obtain this flux.

The best photographs from our previous tests were selected to fix our lighting requirements. Based upon the geometry of the tests and the characteristics of the xenon arc lamp, we first calculated what the level of the illumination was that we had. This gave a value of about 1,000 fc.

To check our calculation, we simulated these test conditions in our laboratory and measured the actual illumination. The results showed that the illumination is not axisymmetric and changes to some extent over the beam width. It generally ranges from about 800 to 900 fc around the periphery to a maximum of 1,100 fc near the lamp axis. These values nicely bracket the calculated value of 1,000 fc.

We wanted to achieve comparable lighting conditions in our new tests. To compute the corresponding value of luminous intensity, the illumination is multiplied by the square of the separation distance. If we assume the same distance as we did before, namely 70', I should be approximately 5×10^6 c.

For our application, it was essential to develop a good understanding of searchlight theory. The only complete reference that we were able to find was the series of papers published by F. Benford in the General Electric Review from 1923 to 1926. Most of his notation will be retained throughout the following review of searchlight optics.

The optical components of a searchlight consist of a parabolic mirror and a light source. The source is located on the mirror axis at the focal point, that is, one focal length F out along the axis in front of the mirror. The coordinates of the mirror are fully determined by F. The maximum angle, though, that the mirror wraps around the source is another important parameter. This angle, which we shall call a*, is measured between two rays from the source, one along the axis to the center of the mirror and the other to the outer edge.

For purposes of analysis, the source is represented as a luminous sphere or disk of radius r. The ratio r/F establishes the beam angle of the searchlight at large distances away. All of the rays reflected by the mirror are parallel to each other in the limit of a point source, $r/F = 0$, and the beam angle is zero. In reality, $r/F \neq 0$. Some divergence is thus unavoidable, but it can be made very small.

Once r/F and a* are fixed, the beam spread and intensity distribution can be calculated at any distance from the searchlight. A "minimum inverse square" distance L_o is identified in these calculations. In the case of a *disk source*[13], which is representative of a monoplane filament lamp, L_o can be calculated from

$$L_o/F = f_1(a^*)/(r/F) \tag{1}$$

where the function $f_1(a^*)$ is given in the Appendix. On the axis beyond L_o, the illumination drops in proportion to the inverse square of the distance from the searchlight. In between, the beam is not fully developed and the variation is less rapid.

The beam shape beyond L_o can be drawn, to a good approximation, as a conical beam with its vertex at the center of the mirror and a total angle determined by

$$C_o = 2 \tan^{-1}(r/F) \tag{2}$$

For C_o to be small, r/F must be small. From Eq. (1), therefore, L_o becomes large. This means in our application that we would be working at distances between the searchlight and L_o. The development of the beam in this region is more complicated. Initially, there is a straight conical section, followed by a break point well before L_o at which the beam enlarges more rapidly. Beyond this break point, the beam edge is curved and approaches asymptotically the conical approximation of Eq. (2).

The coordinates of the beam edge $(L_e, W_e/2)$ can be calculated with the help of the equations,

$$L_e/F = f_2(a)/(r/F) \tag{3}$$

$$(W_e/2)/F = f_3(a) \tag{4}$$

in which the axial distance L_e is measured along the beam axis and the half-width $W_e/2$, normal to it. The functions $f_2(a)$ and $f_3(a)$ are also given in the Appendix and depend on the local mirror angle a which runs from 0 to a*. From these equations, then, the initial straight section of the beam is defined by the outer edge of the mirror and the coordinates obtained with a = a*. The coordinates of the curved boundary are calculated using values of a from 45° down to 0°.

The beam intensity on the axis builds up to a maximum value I* at L_o. Thereafter, it is constant. Between the searchlight and L_o, I can be calculated from the expression,

$$I/I^* = (\tan^2 a/2)/(\tan^2 a^*/2) \qquad (5)$$

Each value of a up to a* corresponds to a distance L from the searchlight computed from Eq. (1) by substitution of a for a* and L for L_o.

In general, I* is specified in beam candles by the searchlight manufacturer. The variation in the illumination E along the beam axis can be determined from the resulting values of I and the relationship

$$E = I/L^2 \qquad (6)$$

Beyond L_o, where I = I*, we see that E is inversely proportional to L^2, as mentioned earlier.

Calculation of the distribution of intensity across the beam is much more complicated and is usually done graphically by means of the procedures detailed in Refs. 14 and 15. For a standard mirror with a* = 60°, the distribution is somewhat peaked at L_o, but it becomes more uniform both toward the searchlight and away from it.

To gain some practical insight, we carried out a sample calculation for the beam spread and the drop in illumination along the axis. A searchlight with r/F = 0.03 and a* = 60° was chosen. With these values, $L_o/F = 102.7$ and the diameter of the beam increases to somewhat less than 1.5 times the mirror diameter at the break point, or 45% of L_o. At L_o, the beam diameter reaches 2.8 times the mirror diameter. Asymptotically, the beam angle becomes 3° 26'. The illumination at 27% of L_o is four times the illumination at L_o and at 57% of L_o, only two times as great.

The sample calculation put us in a good position to evaluate the various commercial searchlights available. Ten companies were contacted. Of these, we narrowed our selection to four companies and compared twelve different designs. Our main considerations were performance, power requirements and cost.

The designs we compared included incandescent, xenon arc and carbon arc types. Most of them had approximately the same performance, except for one xenon arc searchlight. The intensities ranged from 1.55×10^6 c to 7.9×10^6 c, the flux from 146 lm to 9,300 lm and the beam spread from 1.0° to 6.6°.

Two things were immediately clear. The searchlights with incandescent lamps have simple power requirements, combined with a favorable cost. The searchlights with xenon and carbon arc lamps require a d-c power supply and igniter. They cost much more.

The design that we finally picked is the Carlisle & Finch Redundant-D 19" Incandescent Searchlight. This searchlight has a 18 1/8" diameter, silvered

glass reflector with a 7 7/8" focal length. An Alzak spherical, secondary reflector is employed to boost the light output. The power required is 120 v a-c, single phase. The searchlight has a beam intensity I* of 4.26×10^6 c, which is only slightly less than the value we wanted. Inside of L_o, I is smaller than this value, of course, but E is higher than the 1000 fc that we specified because we are closer to the light, see Eq. (6).

The light source itself is a GE 750 w bulb with a rectangular array of filaments in a single plane. The beam, therefore, has a somewhat rectangular shape rather than circular. Based on illumination measurements taken at 126', the beam angle in the horizontal plane is 3° 40' and 3° 30' in the vertical plane.

Taking the 3° 40' beam angle, we calculated an effective value for r/F of 0.032, or slightly larger than we chose for our sample calculation. From the mirror geometry, however, we found a value for a* of 60° which is exactly the same. The value for L_o/F turned out to be 96.2, giving L_o = 63'.

For the total luminous flux, we integrated the illumination measurements furnished us over the beam cross section. This gave a value of 6,590 lm. Since the nominal total output of the lamp is 19,000 lm, the beam efficiency is 34.7% and the overall conversion efficiency is 8.8 lm/w. Both are quite high.

The searchlights, when received, were checked out and met our specifications. As a support, we made up a rectangular frame or yoke from 2" aluminum tubing and fittings. Two diagonal braces, one on each side, extend rearward and outward to hold the frame vertically. The searchlights themselves were held in place within the yoke, utilizing their main mounting lugs and fittings with special sleeves. A photograph of the assembled frame and searchlights is presented in Fig. 4. To allow more flexibility, the feet on the aluminum frame were fastened to a wooden base rather than the tunnel floor.

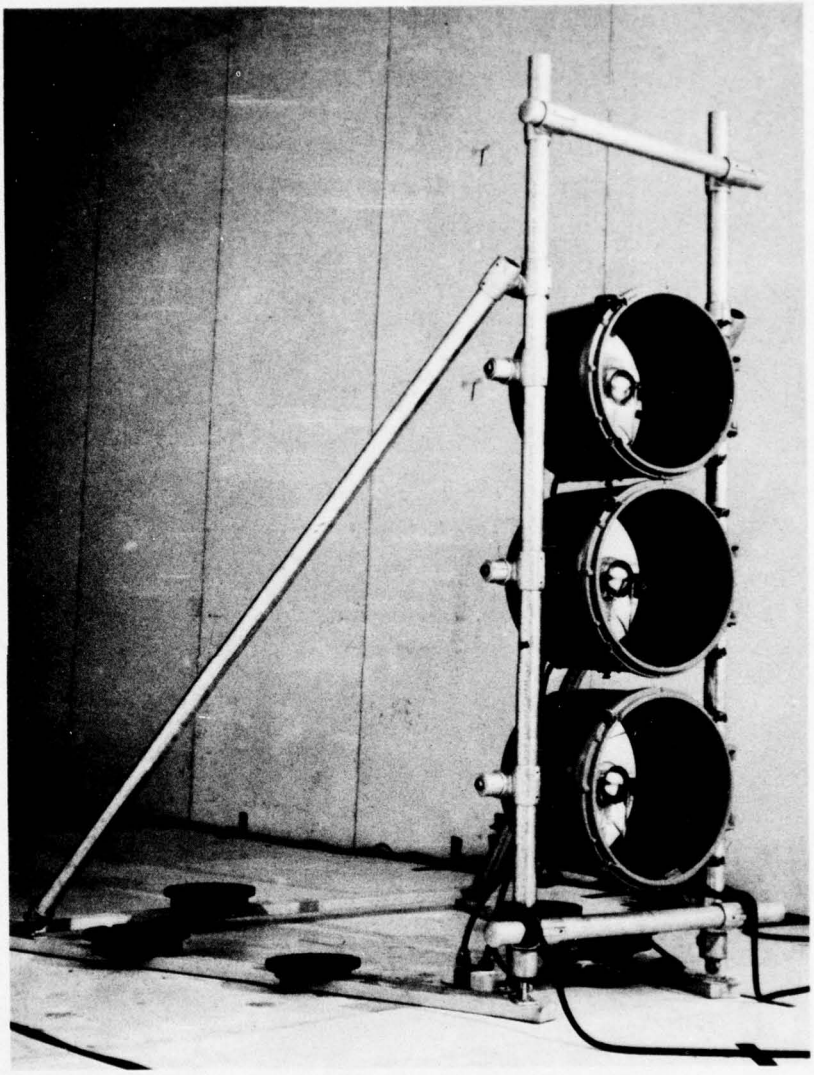

Figure 4. Assembled Frame And Searchlight Array In Wind Tunnel

5 LIGHT CHOPPER

For quantitative data, we constructed and designed a chopper specifically for our purpose. The main element of the chopper is a metal disk with azimuthal slots, equally spaced around the periphery. This disk is placed just ahead of the camera. Light enters the camera in the normal fashion when one of the slots is in front of the lens. Conversely, the light is cut off when the closed area of the disk between slots, or blade, comes in front of the lens. The disk is usually driven directly by a constant speed motor.

The fraction of the time of each on/off cycle during which the lens is *partially* covered we denote by Δ. It is directly proportional to the number of blades n and inversely proportional to the radius R of the center of the camera lens from the axis of rotation. Since n is fixed by the light interruption frequency f desired and the available motor rpm N, the larger the slot radius, the sharper is the cutoff. The power to drive the disk, though, grows rapidly with the disk radius, increasing as the fifth power, as well as with the motor rpm, increasing as the third power.

To design the chopper wheel, we had to determine not only n and R but also the angular width of each blade θ. The following set of equations are convenient in this regard,

$$n = 60f/N \tag{7}$$

$$R = nd/\pi\Delta \tag{8}$$

$$\theta = (\pi/n)(\Delta + 2\gamma) \tag{9}$$

d being the diameter of the camera lens and γ, the fraction of each cycle during which the lens is *totally* covered. The frequency f is expressed in Hz.

A hysteresis synchronous motor was chosen for the disk drive. This type of motor holds its speed precisely, eliminating the need to measure the disk rpm and the possibility of associated errors. We settled upon a motor speed of 3600 rpm and selected a chopping frequency of 240 Hz, based upon our experience with modulation of the xenon arc lamp. From Eq. (7), then, $n = 4$.

For our Rolleiflex camera, $d = 1.13"$. Using this value and taking $\Delta = 0.2$, we got $R = 7.2"$ from Eq. (8). The inner radius of the slots, therefore, was made 6.2" and the outer radius, 8.2". To find θ, we set $\gamma = 0.1$ in Eq. (9). This gave $\theta = 18°$ and each slot was machined out 72° azimuthally.

With the values of Δ and γ assumed, the lens is totally covered for 10% of each

cycle and not covered at all for 70% of each cycle. The actual portion of each cycle over which no bubble image is recorded on the film will fall between 10% and 30%. Where, exactly, depends upon other factors such as the light intensity, camera aperture and film characteristic curve.

Our final design utilizes two of the above disks, sandwiched together, for flexibility. When the slots of the two disks coincide with each other, they act as a single disk. If the disks are displaced rotationally by 18°, the portion of each cycle over which the lens is totally covered increases to 30%. Correspondingly, the portion that the lens is completely uncovered decreases to 50%. The percentage of partial coverage remains the same. Results between these two limits can be achieved by intermediate values of displacement.

The two disks are mounted directly on the motor shaft and clamped into the relative position desired with a hub. A housing surrounds the disks for safety and reduces the aerodynamic torque. We found that a 1/6 hp motor was necessary to drive the disks at synchronous speed with the housing in place. This is about the largest synchronous motor that is manufactured in a convenient and portable size.

The entire unit was attached to an adjustable stand so that we could set it at the proper height and viewing angle. This stand is separate from the camera tripod to avoid transmission of any vibration from the chopper to the camera. A picture of the unit with a different camera in place is shown in Fig. 5.

When the moving bubbles are photographed through the chopper, broken streaks are recorded rather than continuous streaks. If the magnification ratio M of the camera is known, i.e. the ratio of the image size to the object size, the bubble velocity V is easily obtained from

$$V = fs/M \tag{10}$$

where s is the length on the photograph of one complete cycle.

We tested the chopper unit by photographing bubbles in motion through the test section of the SAI 6" x 6" Wind Tunnel. The unit performed very well. Also, the velocity computed from Eq. (10) agreed closely with that measured by a pitot-static probe.

The cutoff of the bubble streaks in each cycle was surprisingly sharp. Originally, we were concerned that the cutoff might not be as well defined as we would like. To overcome this potential problem, we investigated the addition of auxiliary lenses. These lenses would form a real image of the bubbles in the plane of the chopper wheel and a virtual image of the chopper wheel plane at infinity for the camera. We did some limited experiments with simple lenses, but it turned out that a custom design of lenses of much higher quality

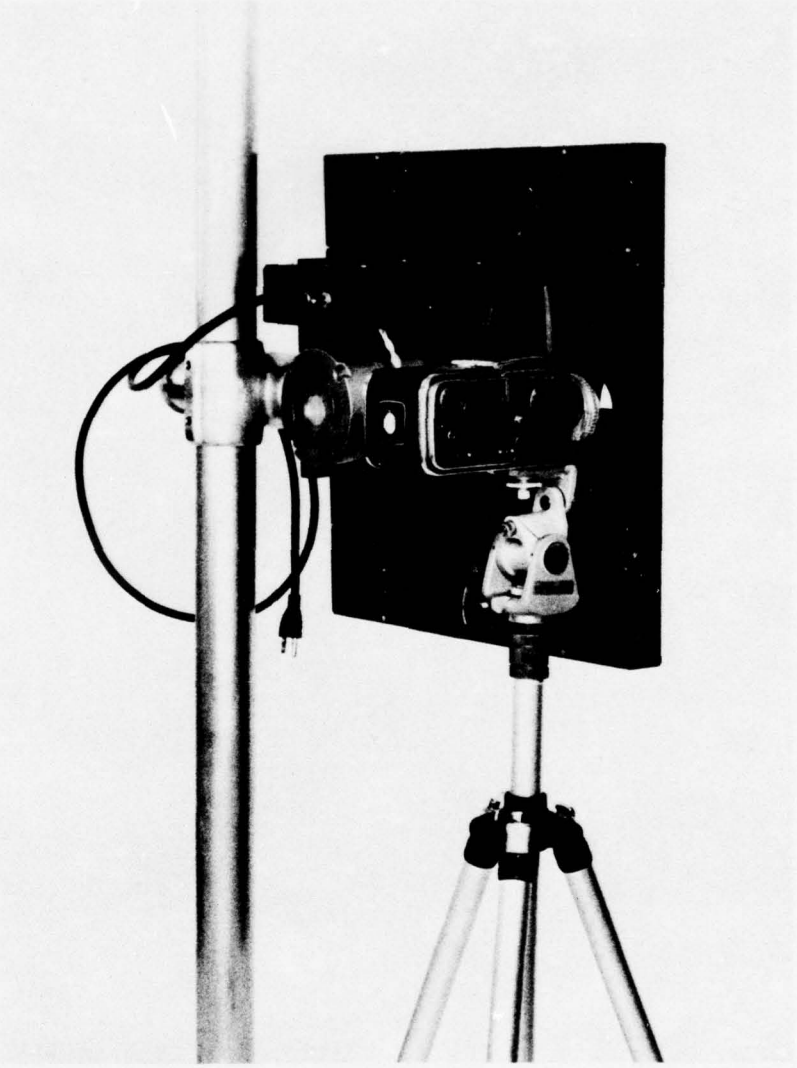

Figure 5. Light Chopper With Hasselblad 500C Camera In Place

was necessary. As a consequence, we abandoned this idea.

6 RECORDING EQUIPMENT

The proper recording equipment and techniques are extremely important. Detailed guidelines are given in Ref. 6. In general, we followed these guidelines and employed a Rolleiflex 2.8C with Kodak Royal-X for our still photographs.

Besides still photographs, we wanted to take motion pictures. Our previous experience with 16 mm movies was not too successful[6]. In particular, we found a number of problems associated with developing, resolution and cost. As an alternative, we investigated the application of video equipment.

Two test trials at speeds up to 200 fps were conducted initially in the SAI 6" x 6" Wind Tunnel. One test trial involved a GBC VF-302 Camera, a Sony VO-1600 3/4" Cartridge Tape Recorder and a Sony CVM-112 11" Monitor/Receiver. The other involved two cameras, a Sony AVC-3210DX and a GBC CTC-5000, a Sony AV-3650 1/2" Reel Recorder and a Sony CVM-112 11" Monitor/Receiver, together with a Sony SEG-1 Special Effects Generator.

The results were remarkable! With modest vidicon tubes in the cameras, the light sensitivity was comparable to the fastest film speeds which we have obtained. Even more striking, the special effects generator permitted negative pictures and simultaneous display of pictures from two cameras. These capabilities greatly facilitate the diagnosis of complex, unsteady airflows.

A third test trial was conducted later with a GE TE-26-S Camera, a Concord VTR 1120 1/2" Reel Recorder, plus an Ampex 5800 1" Reel Recorder, and a GE 12" Monitor/Receiver. A silicon diode vidicon tube was used in the camera. The flow conditions duplicated the conditions of our two prior trials with the GBC and Sony equipment.

Both the live and recorded pictures were outstanding with considerable improvement in definition. Furthermore, the sensitivity now exceeded anything that we had achieved previously. Even a flashlight alone gave sufficient illumination at a speed of 30 fps with an $f/0.78$ lens.

The major components of the final system chosen are a GE 4TE-26-A1C Camera, a Concord VTR 1120 1/2" Recorder and an Electrohome EVM-11 Monitor. The performance of this system was checked out, again by means of the SAI 6" x 6" Wind Tunnel.

There was a problem with the vidicon tube at first. This was traced to the "induction time" for the video signal to build up. The induction time depends upon the light level. Typically, it is about 50 msec, but the induction time was much longer for our tube. Replacement of the tube corrected the problem.

A photograph of the complete system is presented in Fig. 6. The camera and a small viewing monitor are mounted on a tripod at the right. A cart holds the rest of the equipment at the left, the video tape recorder sitting on the lower shelf and the main monitor along with a special effects generator, on the upper shelf. The microphone and amplifier located beside the recorder provide for supplementary sound recording and playback.

Figure 6. Completely Assembled Video System With Equipment Cart And Tripod

7 SELECTION OF WIND TUNNEL

The principal consideration with respect to the selection of a suitable wind tunnel was the length of the test section. Our rotor blade tip model has a chord of 2'. To examine the flowfield up to 20 chords downstream, this means that a length of at least 20' was needed. After a review of the wind tunnels listed in Ref. 16, two candidates were tentatively picked, the NBS Dual Test Section Wind Tunnel and the NASA Langley V/STOL Research Wind Tunnel.

We toured the NBS Tunnel on 16 March and 7 April 1972 to study it more carefully. Two test sections are available. The larger test section is 5' x 7' in cross section with a length just under 40'. Since our model is 5 1/2' in span, the test section height is somewhat marginal if we want to avoid any appreciable effects of wall interference. In addition, the windows for viewing the flow are limited in size and number.

The NASA Langley V/STOL Research Wind Tunnel was visited on 30 August 1972. We felt immediately that this wind tunnel was uniquely qualified for our tests. With a test section 14' high, 21' wide and 50' long, there is no interference problem and the length is more than adequate. The sidewalls and ceiling can also be raised partially or completely, each independent of the others. This configuration affords an unobstructed view of the total flowfield.

Shortly after our visit to the NASA Langley V/STOL Research Wind Tunnel, we submitted a request for approximately 32 hours of occupancy. This request was approved and the tests were conducted over the period from 22 January to 26 January 1973 on a "piggyback" basis. That is, they were run in conjunction with other tests already scheduled when time was available.

8 NASA LANGLEY WIND TUNNEL TESTS AND PRELIMINARY RESULTS

Our test setup in the NASA Langley V/STOL Research Wind Tunnel followed our usual arrangement[6], with the bubble generating heads upstream of the model and the searchlights downstream. To accommodate the ongoing prime test, the rotary sting was left in the tunnel during our tests. We aligned everything, therefore, in a plane approximately midway between the north sidewall and the centerline of the tunnel.

The relative orientation of the bubble generating heads and the model is seen in Fig. 7. The model was positioned immediately behind the tunnel boundary layer removal section in the upstream end of the test section, 5 1/2' in from the north sidewall on the left. It was bolted to the floor at an angle of attack of 8° with the "upper" surface facing the north sidewall. The support rod for the heads was 10' upstream from the model leading edge and 1' closer to the north sidewall.

Three heads were used in the tests, one or more of them operating as desired. They were adjusted vertically and/or horizontally to visualize different portions of the flowfield. The support rod was held by guy wires and the constituents that supply the heads were fed through plastic tubing taped to the tunnel floor and this rod. Black flock paper was put on the heads and support rod to reduce the reflection of light from the searchlights.

The searchlight array was situated approximately 60' downstream of the model as shown in Fig. 8. This photograph gives an overall view of the entire setup and the location of the rotary sting. Actually, the searchlights were in the entrance to the diffuser, placing them well downstream of the portion of the flowfield that we wanted to investigate. All of the photography and videotaping was done from the north side, either through the windows of the sidewall or with the sidewall up.

In the initial shakedown tests, we encountered two minor problems. The south sidewall, painted white, was too bright a background for the still photographs. Consequently, we had to cover it and the sting with sheets of black plastic. On the other hand, the dimly illuminated background enhanced the sensitivity of the video camera to the bubble traces. The second problem concerned the unsteadiness of the flow downstream. With the north sidewall up and the model near the edge of the open jet, the tip vortex apparently entered a region of turbulent mixing downstream. As a result, still photographs of the vortex in the far wake were shot with the sidewall down.

Over the five day test period, the total time of our tunnel occupancy was 24.5 hours. We took some 26 rolls of still photographs, altogether, with 12 expo-

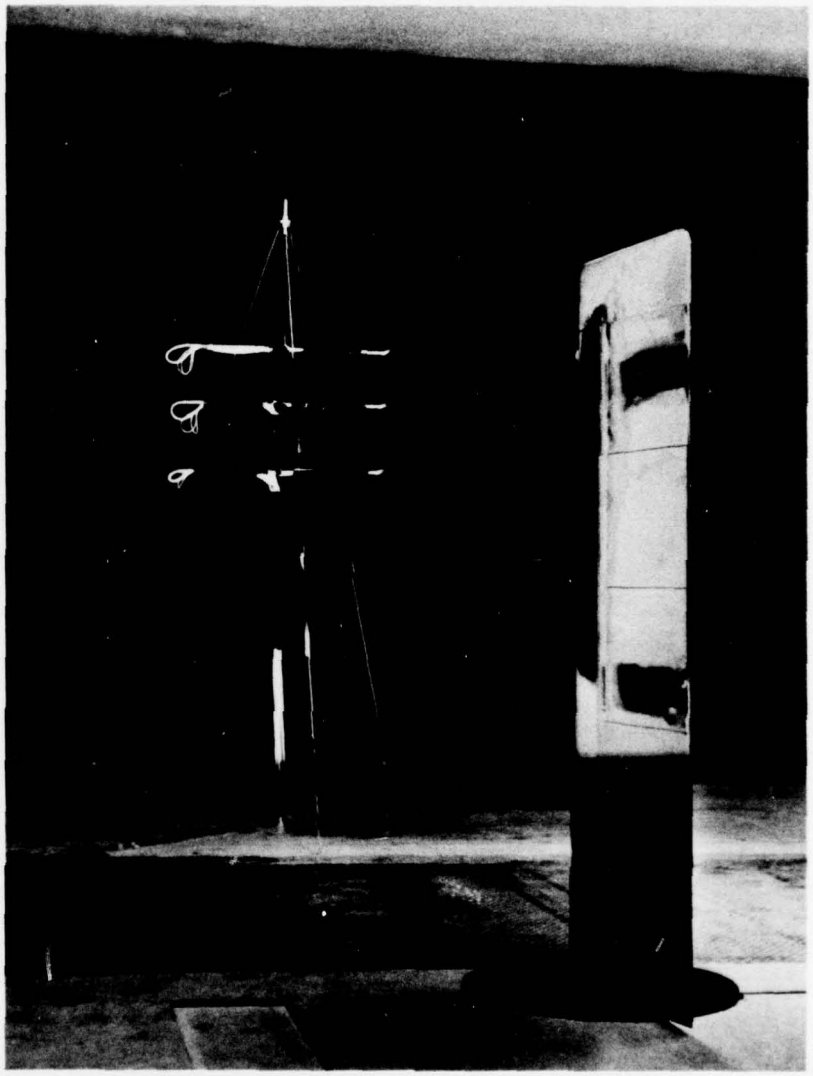

Figure 7. HR2S-1 Helicopter Blade Model And Bubble Generating Heads

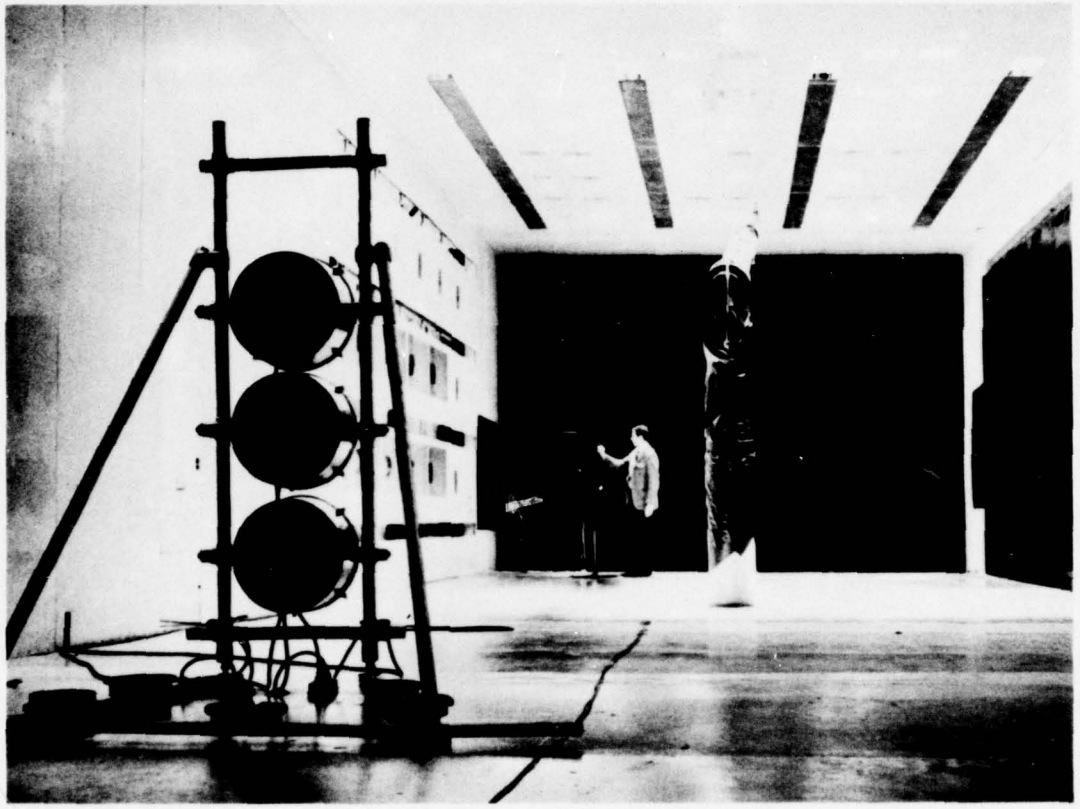

Figure 8. Overall View Of Wind Tunnel Test Setup

sures per roll. Besides these still photographs, we recorded 6 hours of videotape. The test speeds were varied from 20 to 50 fps.

Half of the still photographs were devoted to the far wake with the chopper. The camera view extended from 34' to 40' downstream of the model trailing edge. For these tests, we fixed the tunnel speed at 50 fps. The remaining photographs were taken without the chopper at 20 fps. They covered other portions of the flowfield from a number of different angles.

The extensive videotaping which we did documented almost all of the testing. Especially dramatic is the development of the vortex wake and rollup when the tunnel was started. We also experimented quite successfully with panning the camera to capture a cluster of bubbles as they spiralled around and into the tip vortex.

Some representative still photographs are presented in Figs. 9, 10 and 11. Fig. 9 is a photograph of the details of the flow at the tip of the model and downstream a few chords. It was taken from about 8' away at $f/2.8$ and 1/10 sec. The three heads were operating simultaneously in this case, the middle head feeding bubbles directly into the tip vortex. Note that the bubbles from the upper and lower heads have already begun to wrap around the tip vortex. The wrapping up of the vortex sheet is seen somewhat more clearly in Fig. 10 with the middle head turned off. Otherwise, the photographs are identical. The bubbles which pass "under" the blade, that is around the far side, move rapidly outward compared with the bubbles which pass "over" the blade on the near side. Farther downstream, both groups of bubbles wrapped around the tip vortex in the clockwise direction, facing downstream. Fig. 11 reveals this process beautifully from an oblique angle, looking downward from above the blade tip.

Radial inflow of bubbles into the vortex core is quite evident in Fig. 9. We saw this, too, in the far wake. From the photographs with the chopper, the radial and tangential velocities can be measured as a function of radius. We believe that it is possible to correlate these velocity distributions by means of a suitable mathematical model.

It is uncertain whether the radial inflow of bubbles may be due to a buoyant force on slightly lighter-than-neutrally-buoyant bubbles in the radially-decreasing pressure field of the vortex. To study this, we tried some tests with a smoke generator. The smoke spiralled inwards in the same fashion, convincing us that radial inflow is an essential feature of the tip vortex. The repeatability of our radial velocity data should further increase our confidence in the flow tracing accuracy of the bubbles here.

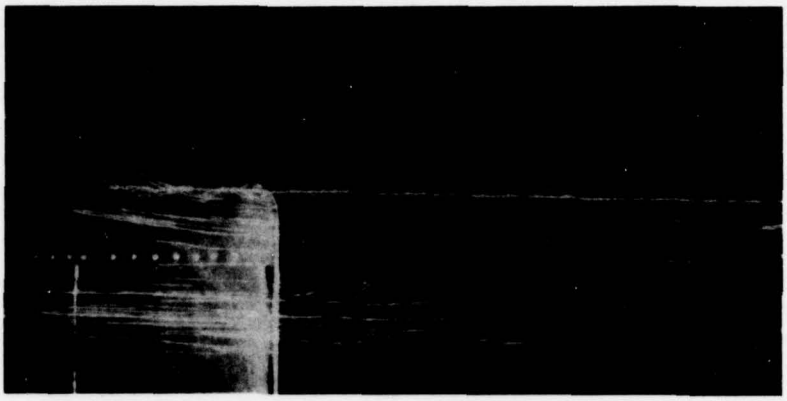

Figure 9. Representative Tip Vortex Flow With Three Heads Operating

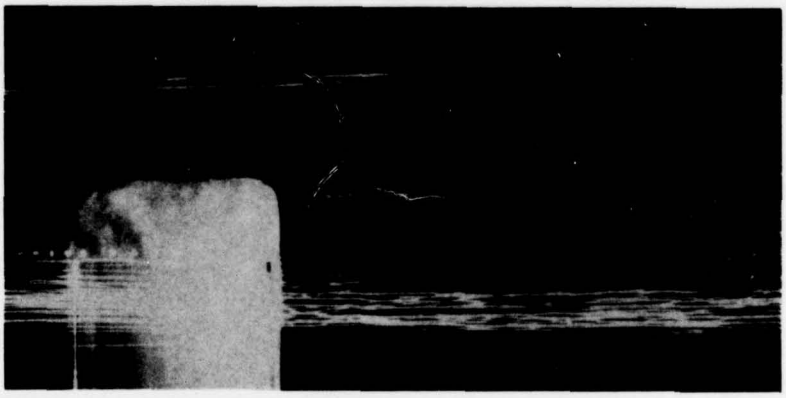

Figure 10. Representative Tip Vortex Flow With Two Heads Operating

Figure 11. Tip Vortex Flow And Development Of Rollup

9 CONCLUSIONS AND RECOMMENDATIONS

An investigation was conducted to examine the tip vortex and total flowfield of a representative helicopter blade model using the helium bubble flow visualization technique. Emphasis was placed on development of a suitable light source and related equipment, plus testing of the model in the NASA Langley V/STOL Research Wind Tunnel. The most important conclusions and recommendations are:

- The searchlight array met the design illumination requirements and proved very satisfactory. Some effort, though, should be made to reduce the secondary illumination which lowers the background contrast.

- The light chopper and multi-head bubble generating rake also met their respective design requirements and proved very satisfactory. A remotely controlled traversing mechanism would greatly facilitate the adjustment of the position of the heads.

- The high-sensitivity video system was an unqualified success. This offers really great promise in flow visualization work, particularly for recording the dynamical aspects of the air motion. It turns out that the background contrast problem is not nearly as severe as for ordinary photography.

- All of the test objectives were achieved. The results reveal many details of the flow, especially the formation of the tip vortex and overall rollup of the vortex sheet which, heretofore, have not been so well defined.

- These tests demonstrated that the helium bubble flow visualization technique has clearly established itself as an indispensable tool for subsonic wind tunnel testing, regardless of the facility size.

- Any tests of tip vortex control devices should include flow observations with this technique. Such observations can quickly show the effectiveness of the device, both at the airfoil and far downstream.

- New subsonic wind tunnels should be designed and existing tunnels modified, where possible, to provide better access for flow visualization work. An open jet is ideal. If this is adopted, however, care must be taken to avoid the turbulent mixing regions along the edges of the jet. It is strongly recommended, too, that all major background surfaces be painted black for maximum bubble visibility.

- Radial inflow was definitely evident in the tests and appears to be a dominant factor in the physical mechanism which sustains the tip vortex, as conjectured. Further reduction of the data and correlation with a mathematical model is required for confirmation.

- To resolve the helicopter problem of vortex blade interaction, flow visualization tests on the tandem blade concept should be pursued. This could lead to substantial increases in static thrust and reduction in blade slap noise.

REFERENCES

1. McCormick, B. W., Aircraft Wakes: A Survey of the Problem, FAA Symposium on Turbulence, Washington, D. C., March 22-24, 1971.

2. ———, Third CAL/AVLABS Symposium on Aerodynamics of Rotary Wing and V/STOL Aircraft, Buffalo, N. Y., June 18-20, 1969.

3. Hale, R. W., Tan, P. and Ordway, D. E., Experimental Investigation of Several Neutrally-Buoyant Bubble Generators for Aerodynamic Flow Visualization, Sage Action, Inc., SAI-RR 6901, August 1969; AD-717 390.

4. ———, Airflow in Wind Tunnel Seen Exactly, Machine Design, Vol. 43, No. 8, p. 12, April 15, 1971.

5. Hale, R. W., Tan, P. and Ordway, D. E., Experimental Investigation of Several Neutrally-Buoyant Bubble Generators for Aerodynamic Flow Visualization, Naval Research Reviews, Vol. XXIV, No. 6, pp. 19-24, June 1971.

6. Hale, R. W., Tan, P., Stowell, R. C. and Ordway, D. E., Development of an Integrated System for Flow Visualization in Air Using Neutrally-Buoyant Bubbles, Sage Action, Inc., SAI-RR 7107, December 1971; AD-756 691.

7. Greenberg, M. D. and Powers, S. R., Nonlinear Actuator Disk Theory and Flow Field Calculations, Including Nonuniform Loading, NASA CR-1672, September 1970.

8. Clark, D. R. and Leiper, A. C., The Free Wake Analysis: A Method for the Prediction of Helicopter Rotor Hovering Performance, Journal of the American Helicopter Society, Vol. 15, No. 1, pp. 3-11, January 1970.

9. Halwes, D. R., Flight Operations to Minimize Noise, VertiFlite, Vol. 17, No. 2, pp. 4-9, February 1971.

10. Piziali, R. and Trenka, A., An Experimental Study of Blade Tip Vortices, Cornell Aeronautical Laboratory, Inc., CAL No. AC-2647-S-1, January 1970.

11. Rosenzweig, M. L., Lewellen, W. S. and Ross, D. H., Confined Vortex Flows with Boundary-Layer Interaction, AIAA Journal, Vol. 2, No. 12, pp. 2127-2134, December 1964.

12. Monnerie, B. and Tognet, A., Effect of the Vortex Springing From a Helicopter Blade Tip on the Flow Around the Next Blade, NASA TT F-14462, February 1972.

13. Benford, F., Studies in the Projection of Light, Part VI, The Parabolic Mirror and Disk Source of Light, General Electric Review, Vol. XXVI, No. 9, pp. 624-631, September 1923.

14. Benford, F., Studies in the Projection of Light, Part VII, Parabolic Mirror and Disk Source of Light (Cont'd), General Electric Review, Vol. XXVI, No. 11, pp. 780-787, November 1923.

15. Benford, F., Studies in the Projection of Light, Part VIII, Parabolic Mirror and Disk Source of Light (Concluded), General Electric Review, Vol. XXVI, No. 12, pp. 818-827, December 1923.

16. Pirrello, C. J., Hardin, R. D., Heckart, M. V. and Brown, K. R., An Inventory of Aeronautical Ground Research Facilities, Volume I - Wind Tunnels, NASA CR-1874, November 1971.

APPENDIX

Listed below are the three functions f_1, f_2 and f_3 used in Eqs. (1), (3) and (4), respectively. These functions, which we have introduced here for convenience, may be obtained by comparison with Ref. 13.

$$f_1 = 2(\tan a^*/2)/(\cos a^*)(\cos^2 a^*/2) \tag{A1}$$

$$f_2 = 1/(\cos^3 a/2)(\sin 3a/2) \tag{A2}$$

$$f_3 = 2 \tan a/2 + (\cos a)/(\cos a/2)(\sin 3a/2) \tag{A3}$$

The arguments a* and a have already been defined in our earlier discussion.

DISTRIBUTION LIST

12	Chief of Naval Research Department of the Navy Arlington, Virginia 22217 Attn: Code 211	(12)
1	Chief of Naval Material/Development Department of the Navy Washington, D. C. 20360 Attn: NAVMAT 0334	(1)
4	Naval Air Systems Command Department of the Navy Washington, D. C. 20360 Attn: NAVAIR 320 NAVAIR 5104 NAVAIR 5301 NAVAIR 53014	(1) (1) (1) (1)
2	Naval Ship Research & Development Center Aviation and Surface Effects Department Bethesda, Maryland 20034 Attn: Head, Code 16 Library, Code 5645	(1) (1)
6	Naval Research Laboratory Department of the Navy Washington, D. C. 20390 Attn: Technical Information Division	(6)
1	U. S. Naval Air Development Center Johnsville, Warminster, Pennsylvania 18974 Attn: Aero Mechanics Department	(1)
1	Superintendent U. S. Naval Postgraduate School Monterey, California 93940	(1)
1	Superintendent U. S. Naval Academy Annapolis, Maryland 21402	(1)
1	Dr. A. L. Slafkosky Scientific Advisor Commandant of the Marine Corps (Code AX) Washington, D. C. 20380	(1)
1	Federal Aviation Agency 800 Independence Avenue, S. W. Washington, D. C. 20553 Attn: Mrs. Joan B. Barriage, AEQ-2	(1)
1	Office of Naval Research Branch Office 495 Summer Street Boston, Massachusetts 02210	(1)
1	Office of Naval Research Branch Office 1030 East Green Street Pasadena, California 91106	(1)

12	Defense Documentation Center Cameron Station, Building 5 Alexandria, Virginia 22314	(12)
1	Office Chief of Research & Development Department of the Army Washington, D. C. 20310 Attn: DARD-ARP-P	(1)
1	U. S. Army Materiel Command Air Systems Division Washington, D. C. 20315 Attn: AMCRD-FA	(1)
1	Director, Headquarters U. S. Army Air Mobility R&D Lab Ames Research Center Moffett Field, California 94035	(1)
1	Director, Ames Directorate U. S. Army Air Mobility R&D Lab Ames Research Center Moffett Field, California 94035	(1)
1	Director, Langley Directorate U. S. Army Air Mobility R&D Lab Langley Research Center Hampton, Virginia 23365	(1)
1	Director, Eustis Directorate U. S. Army Air Mobility R&D Lab Fort Eustis, Virginia 23604	(1)
1	Director, Lewis Directorate U. S. Army Air Mobility R&D Lab Lewis Research Center 21000 Brookpark Road Cleveland, Ohio 44135	(1)
2	U. S. Air Force Flight Dynamics Laboratory Wright-Patterson AFB, Ohio 45433 Attn: PT, Prototype Division FXM, Aeromechanics Branch	(1) (1)
1	Air Force Office of Scientific Research 1400 Wilson Boulevard Arlington, Virginia 22209 Attn: Mr. Milton Rogers	(1)
2	National Aeronautics & Space Administration 600 Independence Avenue, S. W. Washington, D. C. 20546 Attn: Code RAA Code RAV	(1) (1)
1	National Aeronautics & Space Administration Langley Research Center Langley Station, Hampton, Virginia 23365 Attn: Mr. John P. Campbell	(1)
1	National Aeronautics & Space Administration Lewis Research Center Cleveland, Ohio 44135 Attn: Director of Aeronautics	(1)

1 National Aeronautics & Space Administration
Ames Research Center
Moffett Field, California 94035
Attn: Large-Scale Aerodynamics Branch (1)

UNCLASSIFIED

Security Classification

DOCUMENT CONTROL DATA - R & D

(Security classification of title, body of abstract and indexing annotation must be entered when the overall report is classified)

1. ORIGINATING ACTIVITY (Corporate author)	2a. REPORT SECURITY CLASSIFICATION
SAGE ACTION, Inc. P. O. Box 416 Ithaca, New York 14850	Unclassified
	2b. GROUP

3. REPORT TITLE

PRELIMINARY INVESTIGATION OF THE ROLE OF THE TIP VORTEX IN ROTARY WING AERODYNAMICS THROUGH FLOW VISUALIZATION

4. DESCRIPTIVE NOTES (Type of report and inclusive dates)

Technical Report #1, 1 January 1972 - 28 February 1973

5. AUTHOR(S) (First name, middle initial, last name)

R. W. Hale, P. Tan, R. C. Stowell,
L. S. Iwan and D. E. Ordway

6. REPORT DATE	7a. TOTAL NO. OF PAGES	7b. NO. OF REFS
December 1974	36	16

8a. CONTRACT OR GRANT NO.	9a. ORIGINATOR'S REPORT NUMBER(S)
N00014-72-C-0200 b. PROJECT NO.	SAI-RR 7402
c. d.	9b. OTHER REPORT NO(S) (Any other numbers that may be assigned this report)

10. DISTRIBUTION STATEMENT

Approved for public release; distribution unlimited.

11. SUPPLEMENTARY NOTES	12. SPONSORING MILITARY ACTIVITY
	Code 211 Office of Naval Research Arlington, Virginia 22217

13. ABSTRACT

The interaction between the tip vortices and successive rotor blades is responsible for two important helicopter problems, static loss in lift and blade slap during power descent. As a step toward the solution of these problems, the objective of this investigation was to examine the flowfield about an isolated blade in rectilinear flow up to 40 chords downstream. Wind tunnel tests were carried out on the tip section of a HR2S-1 (S-56) blade in the NASA Langley V/STOL Research Wind Tunnel. Visualization of the detailed flow patterns, particularly the tip vortex and rollup in the near wake, was achieved using small, neutrally-buoyant bubbles as flow tracers. To provide adequate illumination, a new, expanded lighting arrangement was assembled from an array of searchlights. Also, a special chopper unit was designed and constructed for quantitative velocity data. Records of the flow patterns were made, both by means of still photography and a video system employing a high-sensitivity camera.

DD FORM 1 NOV 65 1473 (PAGE 1)

S/N 0101-807-6801

UNCLASSIFIED

Security Classification

14. KEY WORDS	LINK A		LINK B		LINK C	
	ROLE	WT	ROLE	WT	ROLE	WT
Helicopter						
Rotor blade aerodynamics						
Tip vortices						
Flow visualization						
Neutrally-buoyant bubbles						
Searchlights						
Light chopper						